Pergamon

Int. J. Solids Structures Vol. 32, No. 17/18, pp. 2547–2570, 1995

0020–7683/95 $9.50 + .00

0020–7683(94)00282–7

ELEMENT-FREE GALERKIN METHODS FOR STATIC AND DYNAMIC FRACTURE

T. BELYTSCHKO, Y. Y. LU, L. GU and M. TABBARA
Departments of Mechanical and Civil Engineering, Robert R. McCormick School of Engineering and Applied Science, Northwestern University, Evanston, IL 60208-3109, U.S.A.

(*Received* 3 *February* 1994)

Abstract—Element-free Galerkin (EFG) methods are presented and applied to static and dynamic fracture problems. EFG methods, which are based on moving least-square (MLS) interpolants, require only nodal data; no element connectivity is needed. The description of the geometry and numerical model of the problem consists only of a set of nodes and a description of exterior boundaries and interior boundaries from any cracks. This makes the method particularly attractive for growing crack problems, since only minimal remeshing is needed to follow crack growth. In moving least-square interpolants, the dependent variable at any point is obtained by minimizing a function in terms of the nodal values of the dependent variable in the domain of influence of the point. Numerical examples involving fatigue crack growth and dynamic crack propagation are presented to illustrate the performance and potential of this method.

1. INTRODUCTION

The element-free Galerkin (EFG) method is a method aimed at the simulation of growing crack problems, both static and dynamic. Its key advantage for this class of problems is that it does not require any element connectivity data and does not suffer much degradation in accuracy when nodal arrangements are irregular. Because of the gridless character of the method, a growing crack can be modeled simply by extending the free surfaces which correspond to the crack. This dramatically simplifies the modeling of moving cracks, for it eliminates the need for remeshing. The method has been demonstrated to be quite successful in elasticity, heat conduction and fatigue crack growth modeling (Belytschko *et al.*, 1993, 1994a,b; Lu *et al.*, 1994a). An alternative formulation of the method was described by Nayroles *et al.* (1992), who called it a diffuse element method.

The gridless character of the EFG method is made possible by the use of moving least-square (MLS) interpolants for the trial and test functions with a variational principle (weak form); see Lancaster and Salkauskas (1981) and Shepard (1968) for descriptions of MLS interpolants. To use MLS interpolants, it is only necessary to construct an array of nodes in the domain under consideration. The method is therefore element free but matches the generality of a finite element method. The key advantages of the EFG method compared with the finite element method are: only a mesh of nodes and a boundary description are needed to develop the discrete equations; the dependent variable and its gradient are continuous in the entire domain, so post-processing to obtain smooth gradient fields, such as strains and stresses, is unnecessary.

One disadvantage of MLS interpolants is that a set of linear algebraic equations must be solved for every spatial point at which the values of the primary dependent variables are to be calculated; see Lancaster and Salkauskas (1981). In order to ameliorate this shortcoming, Lu *et al.* (1994a) used weighted orthogonal basis functions to construct the MLS interpolants. The weighted orthogonal basis functions were obtained by using a Schmidt orthogonalization. By means of these weighted orthogonal basis functions, the burden of inverting the matrix at quadrature points is totally eliminated.

It should be noted that the EFG method differs from other gridless methods, such as the smooth particle hydrodynamics (SPH) method (Lucy, 1977; Gingold and Monaghan, 1977) and the free-Lagrange method (Crowley, 1985; Trease, 1985). In the SPH method,

the basic idea is to use a suitable smooth kernel function that mimics the Dirac delta function. The discrete equations of SPH are then obtained by a collocation process, i.e. by directly applying the partial differential equation at the nodes. The major disadvantage of the SPH method is its poor accuracy. It has been reported that a large number of nodes are usually required in the SPH method to achieve reasonable accuracy in practical applications (Johnson *et al.*, 1993). It was shown by Lu *et al.* (1994b) that the SPH interpolant is almost identical to the EFG method with the Shepard interpolant, i.e. the MLS interpolant with a constant basis. Since the Shepard interpolant uses the constant basis functions, it is not as accurate as the standard finite element method or the EFG method with a linear basis.

The free-Lagrange method also avoids the restrictions of a fixed connectivity between the Lagrangian nodes. Instead, this connectivity in free-Lagrange methods is dynamic in the sense that the nearest neighbors change continually in response to the motion of the nodes. However, to calculate the spatial derivatives and the nodal area (in two dimensions) or nodal volume (in three dimensions), weighted averages of variables over the set of nearest neighbors for each node (point) are used. This requires node connections (e.g. Voronoi meshes) to be established at each time step (or a suitable interval) and hence the free-Lagrange method is not completely gridless. However, the grid is not fixed as in finite element and finite difference methods (Crowley, 1985; Trease, 1985); it can also be thought of as a continuous remeshing scheme.

In the EFG method, a list of nearest neighbors is also required to construct the MLS interpolants. However, nodal connectivities are not needed to obtain the nodal volumes and the gradient fields. In fact, nodal volumes are not required in the EFG formulas, and the gradient fields in the EFG method are consistently calculated by taking the derivatives of the interpolants with respect to spatial variables. Nodal volumes are required in the SPH method, and consistent, accurate schemes for calculating these nodal volumes for arbitrary arrangements of nodes in complicated geometries have not yet been developed.

The attractiveness of meshless methods in treating crack propagation problems lies in their ability to treat them with minimal or no remeshing. By contrast, finite element methods encounter considerable difficulties in treating a moving crack. In static problems, the modeling of crack propagation has been dealt with mainly by remeshing at each step of crack growth [e.g. Wawrzynek and Ingraffea (1987)]. This approach usually requires user intervention and the extension to path-dependent non-linear materials may be quite difficult. Another approach is smeared crack models, where cracking is treated by the constitutive equation by letting the stress in certain directions go to zero as originated by Rashid (1968); the behavior of these models differs significantly from classical fracture mechanics.

For finite element modeling of dynamic crack propagation models, two approaches have been taken. The first is the nodal release technique, where nodes along the crack path are released to model crack extension (Ando *et al.*, 1975; Kobayashi *et al.*, 1976; Yagawa *et al.*, 1977; Malluck and King, 1978; Aoki *et al.*, 1987). This approach has been quite successful but is limited to treating cracks along meshlines. It has been applied almost exclusively to problems of rectilinear crack extension. The second is technique is based on moving meshes, or arbitrary Lagrangian Eulerian formulations, where the mesh is continuously rezoned to accommodate the extension of the crack (Atluri and Nishioka, 1985; Koh *et al.*, 1988). Its application has also been limited to straight cracks.

In this paper, application of the EFG method to static and dynamic fracture problems which involve complex crack paths is described. In Section 2, MLS interpolants are described and in Section 3 the numerical implementation of EFG methods to dynamic problems is given. Numerical results are presented in Section 4 in order to assess the effectiveness of this implementation, and conclusions and discussions are given in Section 5.

2. MOVING LEAST-SQUARE INTERPOLANT

Consider the function $u(\mathbf{x})$ which is defined in the domain Ω. For the arbitrary point $\mathbf{x} \in \Omega$, define $\Omega_{\mathbf{x}}$ as a small domain surrounding the point $\mathbf{x}$ and $\Omega \supset \Omega_{\mathbf{x}}$. For any point $\mathbf{x} \in \Omega_{\mathbf{x}}$, the function $u(\mathbf{x})$ is approximated as

$$u^h(\mathbf{x}) \approx \{1\, x\, y\, x^2 \ldots\} \begin{Bmatrix} a_1(\mathbf{x}) \\ a_2(\mathbf{x}) \\ a_3(\mathbf{x}) \\ \ldots \end{Bmatrix} = \mathbf{p}^{\mathrm{T}}(\mathbf{x})\mathbf{a}(\mathbf{x}) \mathbf{x} \in \Omega_{\mathbf{x}}. \tag{1}$$

Using the MLS technique (Shepard, 1968; Lancaster and Salkauskas, 1981) the coefficients a_i can be obtained by minimizing the following:

$$E[\mathbf{a}(\mathbf{x})] = \sum_{i=1}^{n} w(\mathbf{x}, \mathbf{x}_i)[u_i - u(\mathbf{x}_i)]^2 = \sum_{i=1}^{n} w(\mathbf{x}, \mathbf{x}_i)[\mathbf{u}_i - \mathbf{p}^{\mathrm{T}}(\mathbf{x}_i)\mathbf{a}(\mathbf{x})]^2 \quad \mathbf{x}_i \in \Omega_{\mathbf{x}}. \tag{2}$$

In the above, $w(\mathbf{x}, \mathbf{x}_i)$ is a positive weighting function which decreases as $\|\mathbf{x}_i - \mathbf{x}\|$ increases and $\Omega_{\mathbf{x}}$ is the domain of influence.

Equation (2) can be written in the matrix form:

$$E[\mathbf{a}(\mathbf{x})] = \{\mathbf{u} - \mathbf{P}^{\mathrm{T}}(\mathbf{x}_i)\mathbf{a}(\mathbf{x})\}^{\mathrm{T}}\mathbf{W}(\mathbf{x}, \mathbf{x}_i)\{\mathbf{u} - \mathbf{P}^{\mathrm{T}}(\mathbf{x}_i)\mathbf{a}(\mathbf{x})\}, \tag{3}$$

where $\mathbf{W}(\mathbf{x}, \mathbf{x}_i)$ is an $n \times n$ diagonal matrix and $\mathbf{P}(\mathbf{x}_i)$ is an $m \times n$ matrix, where m is the number of basis functions in $\mathbf{p}(\mathbf{x})$ and n is the number of nodes in $\Omega_{\mathbf{x}}$.

The stationarity of $E(\mathbf{a})$ with respect to $\mathbf{a}$ leads to:

$$\mathbf{A}(\mathbf{x})\mathbf{a}(\mathbf{x}) = \mathbf{B}(\mathbf{x})\mathbf{u}, \tag{4}$$

where

$$\mathbf{A}(\mathbf{x}) = \mathbf{P}^{\mathrm{T}}(\mathbf{x}_i)\mathbf{W}(\mathbf{x}, \mathbf{x}_i)\mathbf{P}(\mathbf{x}_i) \tag{5a}$$

$$\mathbf{B}(\mathbf{x}) = \mathbf{P}^{\mathrm{T}}(\mathbf{x}_i)\mathbf{W}(\mathbf{x}, \mathbf{x}_i). \tag{5b}$$

If $n \geqslant m$ and $\mathbf{A}(\mathbf{x})$ is not singular, we obtain

$$\mathbf{a}(\mathbf{x}) = \mathbf{A}^{-1}(\mathbf{x})\mathbf{B}(\mathbf{x})\mathbf{u}, \tag{6}$$

and substituting eqn (6) into eqn (1), gives

$$u^h(\mathbf{x}) = \mathbf{p}^{\mathrm{T}}(\mathbf{x})\mathbf{A}^{-1}(\mathbf{x})\mathbf{B}(\mathbf{x})\mathbf{u} = \sum_{I}^{n}\sum_{j}^{m} p_j(\mathbf{x})(\mathbf{A}^{-1}(\mathbf{x})\mathbf{B}(\mathbf{x}))_{jI}u_I \equiv \sum_{I}^{n} \phi_I(\mathbf{x})u_I, \tag{7}$$

where the shape function $\phi_I(\mathbf{x})$ is defined by

$$\phi_I(\mathbf{x}) = \sum_{j}^{m} p_j(\mathbf{x})(\mathbf{A}^{-1}(\mathbf{x})\mathbf{B}(\mathbf{x}))_{jI}. \tag{8}$$

Equation (7) is the MLS interpolant for $u(\mathbf{x})$. An estimate of the derivative of a function $u(\mathbf{x})$ at any point $\mathbf{x} \in \Omega$ can be obtained by considering $\mathbf{a}(\mathbf{x})$ as a constant (Nayroles *et al.*, 1992)

$$\frac{\partial u^h}{\partial x} \approx \mathbf{p}_{,x}(\mathbf{x})\mathbf{a}(\mathbf{x}). \tag{9}$$

Belytschko *et al.* (1994b) recommended a more accurate formula to calculate $u^h_{,x}$. This formula for $u^h_{,i}$ will give better results, as shown in their paper. It is given by

$$u_{,i}^h(\mathbf{x}) = \sum_I^n \phi_{I,i}(\mathbf{x}) u_I = \sum_j^m \{p_{j,i}(\mathbf{A}^{-1}\mathbf{B})_{jI} + p_j(\mathbf{A}_{,i}^{-1}\mathbf{B} + \mathbf{A}^{-1}\mathbf{B}_{,i})_{jI}\} u_I, \tag{10}$$

where

$$\mathbf{A}_{,i}^{-1} = -\mathbf{A}^{-1}\mathbf{A}_{,i}\mathbf{A}^{-1} \tag{11}$$

and the index following a comma denotes a spatial derivative with respect to x_i (i.e. $x_1 = x$ and $x_2 = y$).

In this paper, the exponential weight function with $k = 1$ given by Belytschko *et al.* (1994b) is used, which is

$$w_I(d_I^{2k}) = \begin{cases} \dfrac{e^{-(d_I/c)^{2k}} - e^{-(d_{mI}/c)^{2k}}}{(1 - e^{-(d_{mI}/c)^{2k}})} & \text{if } d_I \leqslant d_{mI} \\ = 0 & \text{if } d_I > d_{mI} \end{cases} \tag{12}$$

$$d_I = \|\mathbf{x} - \mathbf{x}_I\|, \tag{13}$$

where c is a constant which controls the relative weights and d_{mI} is the domain of the support for the weight function $w_I(d_I^{2k})$. This domain, where $w_I(\mathbf{x})$ is non-zero, is often called the domain of influence of node $\mathbf{x}_I$. It was shown by Belytschko *et al.* (1994b) that the derivatives of the above weight function with respect to x or y exist to any desired order if k is a positive integer. Moreover, it was found that the above weight function, which is essentially a truncated Gauss distribution, performs far better than a conical weight function. In the latter, the results are more sensitive to the value of d_{mI}.

A theory for an optimal value of c is not available. We have used the procedure given by Belytschko *et al.* (1994b):

$$c = \alpha c_I, \tag{14}$$

where

$$c_I = \max_{J \in S_J} \|\mathbf{x}_J - \mathbf{x}_I\| = \max_{J \in S_J} D_J(\mathbf{x}_I). \tag{15}$$

We have used $1 \leqslant \alpha \leqslant 2$, and $\alpha = 1$ for problems with singularities and high gradients. In the above, $D_J(\mathbf{x}_I)$ is the distance between points $\mathbf{x}_I$ and $\mathbf{x}_J$ and S_J is the minimum set of neighboring points of $\mathbf{x}_I$ which construct a polygon surrounding $\mathbf{x}_I$. In the case where the nodes are randomly distributed but the integration cells are uniformly distributed, c_I can be defined as a characteristic length of the integration zone (or cell) that contains the point $\mathbf{x}_I$.

It is not trivial to construct a polygon surrounding each node $\mathbf{x}_I$. Instead the ith smallest distance can be used (Lu *et al.*, 1994b), i.e.

$$c_I = D_i(\mathbf{x}_I) \quad \text{for all } J \text{ but } J \neq I, \tag{16}$$

where D_i is the list of distances sorted in increasing order. For example, we can choose the fourth smallest distance, which is equivalent to c_I defined in eqn (15) for regularly distributed nodes. The ith smallest distance can easily be found by using the median method (Cormen *et al.*, 1990). If we have a total of $N+1$ nodes, the median method gives the ith smallest distance for a given node $\mathbf{x}_I$ by recursively partitioning the remaining N nodes, and the running time is $O(N)$ in the worst case. Here the notation $O()$ denotes the asymptotic upper bound. The drawback of the definition (16) is that communication between nodes can be

lost in some cases if d_{mI} is not large enough. However, this difficulty can be alleviated by finding the total i smallest distances in the i directions.

3. NUMERICAL IMPLEMENTATION

3.1. *Weak form*

We consider the transient response of a non-linear solid but restrict ourselves to small displacements for simplicity. The solid occupies the domain Ω bounded by Γ. The conservation of momentum gives

$$\nabla \cdot \boldsymbol{\sigma} + \mathbf{b} = \rho \mathbf{a} \quad \text{in } \Omega, \tag{17}$$

where $\boldsymbol{\sigma}$ is the stress tensor, which corresponds to the displacement field $\mathbf{u}$; $\mathbf{v} := \dot{\mathbf{u}}$ and $\mathbf{a} := \dot{\mathbf{v}}$ are the velocity and acceleration, respectively; $\mathbf{b}$ is a body force vector and ρ is the density. The initial value problem consists of finding the displacement $\mathbf{u}$ which satisfies eqn (17) and the following initial conditions:

$$\mathbf{u}(\mathbf{x}, 0) = \mathbf{u}_0(\mathbf{x}, 0) \quad \text{in } \Omega \tag{18a}$$

$$\mathbf{v}(\mathbf{x}, 0) = \mathbf{v}_0(\mathbf{x}, 0) \quad \text{in } \Omega \tag{18b}$$

and boundary conditions:

$$\boldsymbol{\sigma} \cdot \mathbf{n} = \bar{\mathbf{t}} \quad \text{on } \Gamma_t \tag{19a}$$

$$\mathbf{u} = \bar{\mathbf{u}} \quad \text{on } \Gamma_u, \tag{19b}$$

where the overbar denotes prescribed boundary values, $\mathbf{u}_0(\mathbf{x}, 0)$ and $\mathbf{v}_0(\mathbf{x}, 0)$ are the initial displacement and velocity respectively and $\mathbf{n}$ is the unit normal to the domain Ω.

The weak forms corresponding to the above equations are given as follows. Consider test functions $\delta\mathbf{w}(\mathbf{x}, t) \in H^1$ and trial functions $\mathbf{u}(\mathbf{x}, t) \in H^1$. Then if

$$\int_\Omega \delta\mathbf{w} \cdot \rho\mathbf{a}\, d\Omega + \int_\Omega \nabla_s \delta\mathbf{w} : \boldsymbol{\sigma}\, d\Omega - \int_\Omega \delta\mathbf{w} \cdot \mathbf{b}\, d\Omega - \int_{\Gamma_t} \delta\mathbf{w} \cdot \bar{\mathbf{t}}\, d\Gamma = 0 \quad \forall \delta\mathbf{w} \in H^1 \tag{20}$$

$$\int_\Omega \delta\mathbf{w} \cdot \rho\mathbf{u}(\mathbf{x}, 0)\, d\Omega = \int_\Omega \delta\mathbf{w} \cdot \rho\mathbf{u}_0(\mathbf{x}, 0)\, d\Omega \quad \forall \delta\mathbf{w} \in H^1 \tag{21a}$$

$$\int_\Omega \delta\mathbf{w} \cdot \rho\mathbf{v}(\mathbf{x}, 0)\, d\Omega = \int_\Omega \delta\mathbf{w} \cdot \rho\mathbf{v}_0(\mathbf{x}, 0)\, d\Omega \quad \forall \delta\mathbf{w} \in H^1 \tag{21b}$$

$$\int_{\Omega_u} \delta\mathbf{w} \cdot \rho\mathbf{u}\, d\Gamma = \int_{\Gamma_u} \delta\mathbf{w} \cdot \rho\bar{\mathbf{u}}\, d\Gamma \quad \forall \delta\mathbf{w} \in H^1 \tag{22}$$

then eqns (17)–(19) are satisfied. In the above, $\nabla_s \mathbf{w}$ is the symmetric part of $\nabla\mathbf{w}$ and H^1 and H^0 denote the Sobolev spaces of degree one and zero, respectively. Equation (20) is the weak form of the equation of motion (17) and the natural boundary condition (19a), eqn (21) is the weak form of the initial condition (18) (see Hughes, 1987), and eqn (22) is the weak form of the essential boundary condition (WFEBC) (19b).

In the finite element method, the shape function satisfies

$$\phi_I(\mathbf{x}_J) = \delta_{IJ}, \tag{23}$$

so most essential boundary conditions can easily be applied; for example, the homogeneous

essential boundary condition can be applied by simply setting the corresponding nodal values to zero. In the EFG method, the imposition of the essential boundary conditions is more difficult since the shape function given in eqn (7) does not satisfy eqn (23). The weak form of the essential boundary condition (22) provides one way of imposing the essential boundary conditions. Alternative methods for enforcing the essential boundary condition, such as Lagrange multipliers, modified variational principles and boundary collocation have been studied by Belytschko *et al.* (1993, 1994a,b) and Lu *et al.* (1994a).

In this paper, the weak forms given in eqns (21) and (22) are used. For static problems, it can be shown that the discrete equations obtained by using the weak form of the essential boundary condition (22) is identical to that obtained by Lagrange multipliers as long as the shape functions for the Lagrange multipliers are chosen to be the same as the trial and test functions; see Lu *et al.* (1994b). In the approach described in the latter, the shape functions given in eqn (17) are modified by taking into account the weak form of the essential boundary condition (22).

3.2. *Discrete equations*

The discretization process for the EFG method parallels that for finite elements, for as indicated above, the only major difference is the fact that the trial functions do not satisfy the essential boundary conditions. We now consider linear elasticity where

$$\boldsymbol{\varepsilon} = \nabla_s \mathbf{u} \tag{24}$$

$$\boldsymbol{\sigma} = \mathbf{D}\boldsymbol{\varepsilon}. \tag{25}$$

In order to obtain the discrete equation from the weak form (20), the approximate solution $\mathbf{u}$ and the test function $\delta\mathbf{w}$ are constructed according to the modified shape function which satisfies the essential boundary condition in the sense of weak form (Lu *et al.* 1994b). The final discrete equations can be obtained by substituting the trial functions and test functions into the weak form (20), which yields

$$\mathbf{M}\mathbf{a} + \mathbf{f}^{\text{int}} = \mathbf{f}^{\text{ext}} \tag{26}$$

$$\mathbf{M}\mathbf{u} = \mathbf{u}_0 \quad \text{at } t = 0 \tag{27}$$

$$\mathbf{M}\mathbf{v} = \mathbf{v}_0 \quad \text{at } t = 0 \tag{28}$$

where $\mathbf{M}$, $\mathbf{f}^{\text{int}}$ and $\mathbf{f}^{\text{ext}}$ consist of 2×2 submatrices $\mathbf{M}_{IJ}$ and 2×1 submatrices $\mathbf{f}_I^{\text{int}}$ and $\mathbf{f}_I^{\text{ext}}$ given by

$$\mathbf{M}_{IJ} = \int_\Omega \rho\phi_I\phi_J\mathbf{I}\,d\Omega \tag{29}$$

$$\mathbf{f}_I^{\text{int}} = \int_\Omega \mathbf{B}_I^{\mathrm{T}}\boldsymbol{\sigma}\,d\Omega \tag{30a}$$

$$\mathbf{f}_I^{\text{ext}} = \int_{\Gamma_t} \phi_I\bar{\mathbf{t}}\,d\Gamma + \int_\Omega \phi_I\mathbf{b}\,d\Omega - \int_\Omega \phi_I\rho\ddot{\mathbf{f}}^*\,d\Omega - \int_\Omega \mathbf{B}_I^{\mathrm{T}}\mathbf{D}\mathbf{F}\,d\Omega \tag{30b}$$

$$\mathbf{u}_{0I} = \int_\Omega \rho\phi_I\mathbf{u}_0(\mathbf{x},0)\,d\Omega \tag{31a}$$

$$\mathbf{v}_{0I} = \int_\Omega \rho\phi_I\mathbf{v}_0(\mathbf{x},0)\,d\Omega, \tag{31b}$$

where

$$\mathbf{B}_I = \begin{bmatrix} \phi_{I,x} & 0 \\ 0 & \phi_{I,y} \\ \phi_{I,y} & \phi_{I,x} \end{bmatrix} \tag{32a}$$

$$\mathbf{F} = \begin{bmatrix} f^*_{1,x} \\ f^*_{2,y} \\ f^*_{1,y} + f^*_{2,x} \end{bmatrix}, \tag{32b}$$

where $\mathbf{I}$ in eqn (32a) is a 2×2 unit matrix. The shape function ϕ_I in eqns (29)–(32) has been modified according to the weak form of the essential boundary condition (19b) and the vector $\mathbf{f}^*$ is due to this modification; see Lu *et al.* (1994b).

In order to perform the integrations in eqns (29)–(31), an extension of the cell scheme proposed by Belytschko *et al.* (1994) is used. The cells are independent of the nodes and are arranged in a regular pattern in both dimensions. In forming the discrete equations, each cell is considered in turn and Gaussian quadrature is performed. Each quadrature point contributes non-zero entries to the equations only to those nodes which are in its domain of influence. Thus, in the final equations, no coupling occurs between nodes which are not within a specified distance (which corresponds to the domain of influence). If the nodes are numbered judiciously, for example by sorting the **x**-coordinates, the equations will be banded.

3.3. *Time integration*

The initial value problem consists of finding the displacement $\mathbf{u}$ which satisfies the semidiscrete equation (26) and the initial conditions (27) and (28). The most widely used methods of direct time integration for solving eqn (32) is the Newmark β-integrator. In this paper, the average acceleration method, which is a special case of the Newmark β-integrator, is used for implicit time integration and the central difference method is used for the explicit time integration, i.e. we have:

average acceleration method (implicit method):

$$\mathbf{u}^{n+1} = \mathbf{u}^n + \Delta t \mathbf{v}^n + \frac{(\Delta t)^2}{4}(\mathbf{a}^n + \mathbf{a}^{n+1}) \tag{33a}$$

$$\mathbf{v}^{n+1} = \mathbf{v}^n + \frac{\Delta t}{2}(\mathbf{a}^n + \mathbf{a}^{n+1}); \tag{33b}$$

central difference method (explicit method):

$$\mathbf{u}^{n+1} = \mathbf{u}^n + \Delta t \mathbf{v}^{n+1/2} \tag{34a}$$

$$\mathbf{v}^{n+1/2} = \mathbf{v}^{n-1/2} + \Delta t \mathbf{a}^n, \tag{34b}$$

where Δt is the time increment and the superscript designates the time step.

The algorithms (33) and (34) are unconditionally stable and conditionally stable, respectively (Lu *et al.* 1994b). The stability condition for algorithm (34) is given by

$$\Delta t \omega_{\max} \leqslant 2, \tag{35}$$

where $\omega_{\max} = (\lambda_{\max})^{1/2}$ and $\lambda_{\max}$ is the maximum eigenvalue of

$$\mathbf{K}\mathbf{x} = \lambda\mathbf{M}\mathbf{x}. \tag{36}$$

It is generally awkward to determine the maximum eigenvalue by solving the above eigenvalue problem. Nevertheless, upper bounds can easily be found from the Gerschgorin theorem (Lancaster and Tismenetsky, 1985) which states:

$$\lambda_{\max} \leqslant \max_{1 \leqslant i \leqslant n} \sum_{j}^{n} |M_{ik}^{-1} K_{kj}| = \|\mathbf{M}^{-1}\mathbf{K}\|_{\infty}, \tag{37}$$

where n is the order of matrices $\mathbf{K}$ and $\mathbf{M}$.

4. NUMERICAL RESULTS

In this section, several static and dynamic fracture problems are considered to evaluate the effectiveness of the method for this class of problem. Of particular interest in these examples is the effectiveness of various ways of meshing the near-tip crack zone and how these strategies are affected by whether the problem is static or dynamic. The latter is of relevance because the governing equations are elliptic and hyperbolic, respectively, for the static and dynamic equations of elasticity.

The first set of examples are static, elastic problems which examine the ability of EFG to model near-tip stress fields and compute stress intensity factors. The first problem consists of a square domain with one free boundary from which an edge crack emanates as shown in Fig. 1. At the remaining three boundaries the tractions corresponding to the exact solution for the near-tip crack field are applied. Thus the near-tip stress field is an exact solution to this problem and the convergence behavior of EFG in the presence of a crack tip can be studied by means of this problem.

The meshes shown in Fig. 2 were used for the study. Linear basis functions were used for the EFG interpolants. c_I was calculated by using eqn (16) with the fourth smallest distance for a given node; $d_{mI} = 3c$ and $c = c_I$ was used in the calculation. The L2 norms of the error in the energy are shown in Fig. 3; the abscissa for the meshes c and d corresponds to an estimate of where a corresponding rectangular mesh would lie for the same number of degrees of freedom. In Fig. 3, quadrature A means that 5×5 Gauss quadrature was used in the region with 14×5 cells and 5×5 Gauss quadrature was used in the rest of the regions; quadratures B, C and D indicate that 3×3, 5×5 and 7×7 Gauss quadratures were used in all cells, respectively. For the uniform meshes such as mesh a and mesh b shown in Fig. 2, the cell structures were equivalent to these meshes and 3×3 Gauss quadrature was used in all cells. It was found that the results obtained by using 3×3 and 5×5 Gauss quadratures are the same for the uniform meshes in this case. It can be seen that the rectangular meshes exhibit a rate of convergence of 0.519, but that for a given number of degrees of freedom the radial mesh gives better accuracy.

The stress distributions for mesh c are shown in Fig. 4, along with the exact solutions for these stresses; the contour plots are displaced by skipping the crack tip to avoid the singularity at the crack tip. It can be seen that the stress fields in the EFG closely replicate the exact solution for mesh c. Furthermore, in contrast to finite element solutions for the stresses, the EFG stresses are continuous. The EFG solution exhibits some aliasing, i.e. wiggles near the crack tip. This aliasing is more pronounced for coarse meshes and is an effective indicator of insufficient resolution. For example, aliasing is very pronounced in the coarse rectangular mesh solution, as shown in Fig. 5.

One idiosyncrasy of the EFG method we have noticed is that the stress intensity factor as evaluated by the method is more domain-dependent than in the finite element method. For example, the stress intensity factor for the edge crack problem shown in Fig. 6 was evaluated using various rectangular domains using domain integrals (Li *et al.*, 1985; Moran and Shih, 1987a,b). In Fig. 7, the values of the mode I stress intensity factor as a function

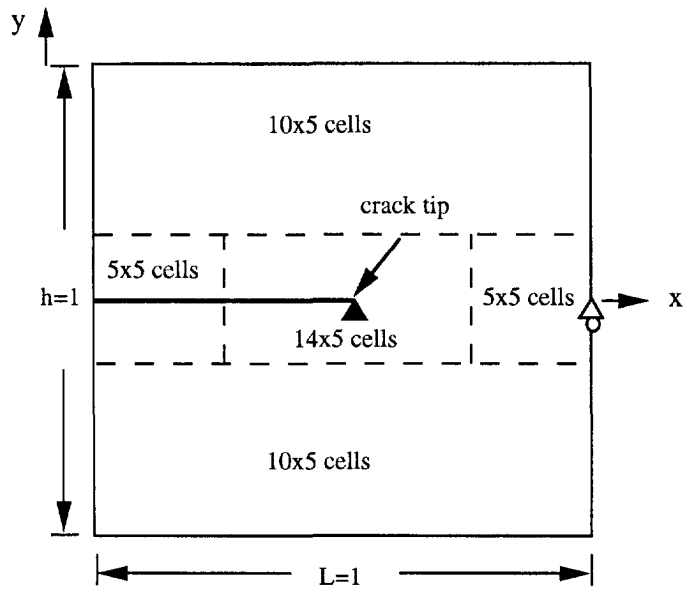

(a)

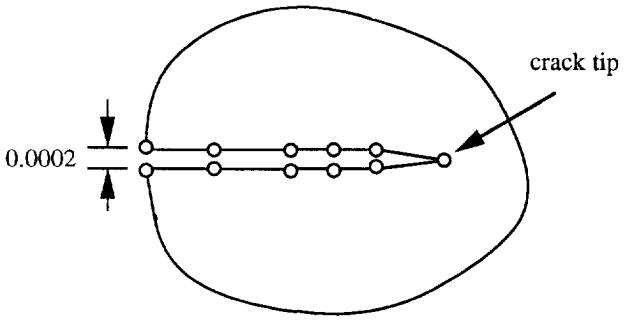

(b)

Fig. 1. (a) Statement for the near-tip crack problem and the cell structures used for mesh c; (b) after the crack passes through a node, each node is replaced by two nodes which are placed normal to the crack surface a distance 0.0001 from the crack.

of the size of the domain are compared with those obtained with a finite element solution. The number of cells was 10×10 as shown in Fig. 6(a). To evaluate the integrals in the weak form, eqn (30), 3×3 Gauss quadrature was used in all cells except the two around the crack tip, where 7×7 Gauss quadrature was used. It can be seen that for the finite element solution, the extracted stress intensity factor is independent of the size of the domain once it exceeds a critical minimum radius. On the other hand, the stress intensity factors computed by EFG exhibit some domain dependence, particularly for the coarser mesh. We have no explanation for this difference at this time.

It is also noted that in the solution of the near-tip crack problem, it is more difficult to obtain an accurate computation of the stress intensity factor than in the edge crack problem. In the edge crack problem, the mesh shown in Fig. 6(c) suffices to obtain 0.2% accuracy in

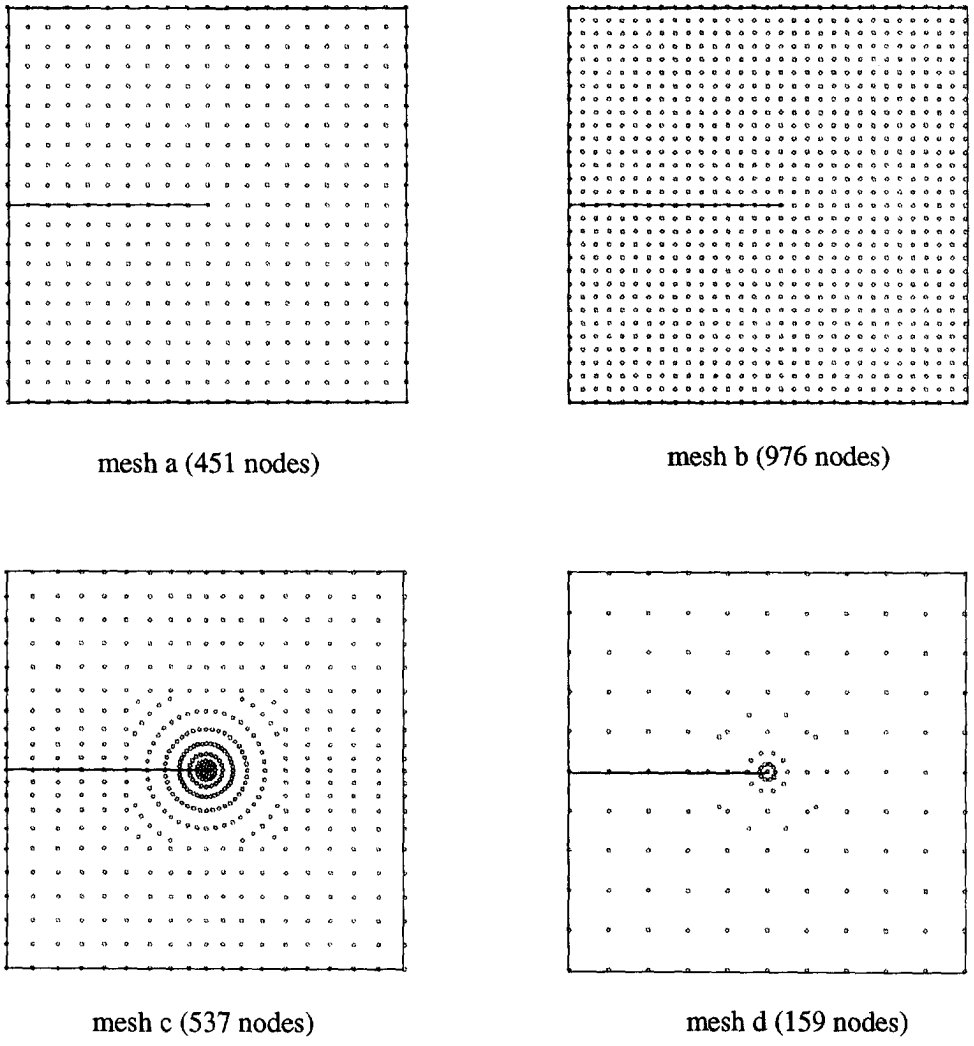

Fig. 2. Meshes for the near-tip crack problem.

K_I. On the other hand, in the near-tip crack field problem, for the meshes c and d shown in Fig. 2, the errors in K_I are 4.5 and 1.4%, respectively.

The second group of examples concern fatigue growth of cracks emanating from holes in a square plate loaded in tension as shown in Fig. 8. The crack growth is assumed to be governed by the Paris–Erdogan law, so that the extension of the crack in dN load cycles is given by

$$da = C\{\Delta K_{eq}\}^n \, dN, \tag{38}$$

where C and n are primarily material parameters but can also depend on environmental effects, and ΔK_{eq} is the range of equivalent mode I stress intensity factors, i.e.

$$\Delta K_{eq} = K_{eq}^{max} - K_{eq}^{min}, \tag{39}$$

where K_{eq}^{min} and K_{eq}^{max} are the minimum and maximum equivalent mode I stress intensity factors associated with the minimum and maximum cyclic applied loads, respectively.

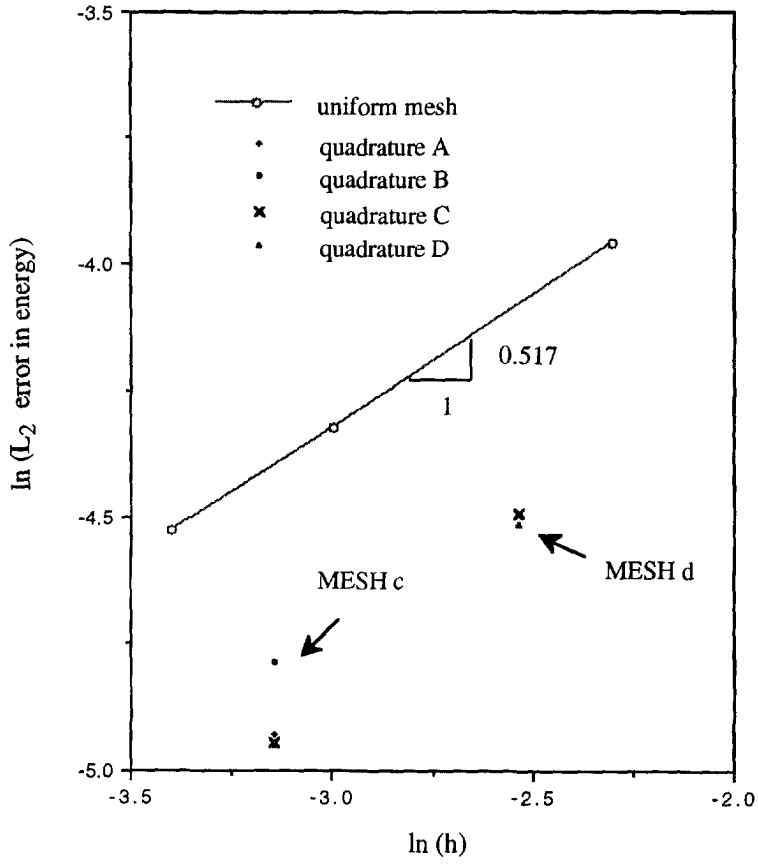

Fig. 3. Convergence rates in energy-norm for the near-tip mixed-mode crack problem.

Since fatigue laws are generally based on an equivalent mode I case to simulate actual mixed mode behavior, the following equation for ΔK_{eq} is used (Broek, 1982):

$$\Delta K_{eq} = \Delta K_I \cos^3 \frac{\theta}{2} - 3\Delta K_{II} \cos^2 \frac{\theta}{2} \sin \frac{\theta}{2}, \tag{40}$$

where ΔK_I and ΔK_{II} are the range of mode I and mode II stress intensity factors, respectively. The crack growth direction depends on the material properties and the history of the loading and crack path. The experimental observations (Smith and Wiersma, 1986; Bazzard *et al.*, 1986) show that the preferable crack path is the direction where $K_{II} = 0$. Many mixed-mode fracture initiation theories have been proposed. The representative theories are: (1) the maximum circumferential stress theory (Erdogan and Sih, 1963); (2) the maximum energy release rate theory (Hussain *et al.*, 1974); and (3) the minimum strain energy density theory (Sih, 1974). In the current study, the maximum circumferential stress theory has been used. The direction of crack growth measured from the current crack line, θ, is determined from (Erdogan and Sih, 1963)

$$\Delta K_I \sin\theta + \Delta K_{II}(3\cos\theta - 1) = 0. \tag{41}$$

Equation (41) can be solved by an iterative approach such as Newton's method.

Since the growth of the crack is monotonic, the crack length was incremented by a fixed increment Δa in each step; furthermore, within each step the crack growth was assumed to be unidirectional. These assumptions are of course tenable only if the increments

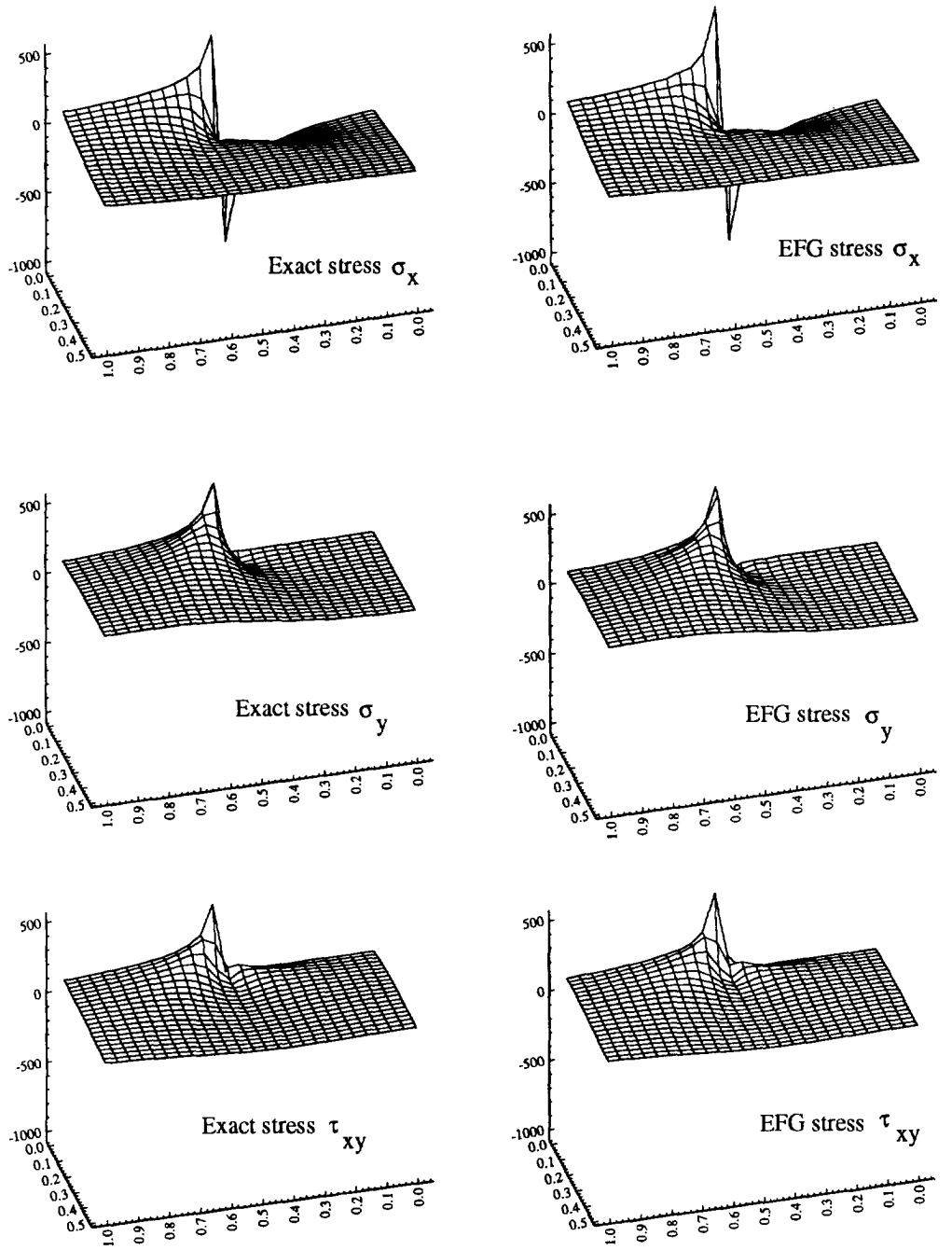

Fig. 4. Stress distributions ($y > 0$) for mesh c in the near-tip mixed-mode crack problem.

are small enough to make the errors due to these assumptions small. These calculations are quite preliminary, and we have not examined carefully the errors arising from the step size which was chosen, although, as we shall indicate, in certain stages of the calculation, they were probably excessive; we are now working on procedures where the crack growth increment is governed by the consequent changes in the stress field.

Crack growth for these models was simulated for two initial angles of the crack: $\theta = 10^\circ$ and 45°, with initial crack lengths of 0.2. In both cases, the length and angle of the initial crack are identical, which is physically quite unrealistic, but serves to simplify the model, since the growth of each crack at each step is then also identical. The cell structure for the crack with $\theta = 10^\circ$ is shown in Fig. 9, along with the nodal arrangements used in the steps which are shown. A total of nine steps was used. The striking feature of this

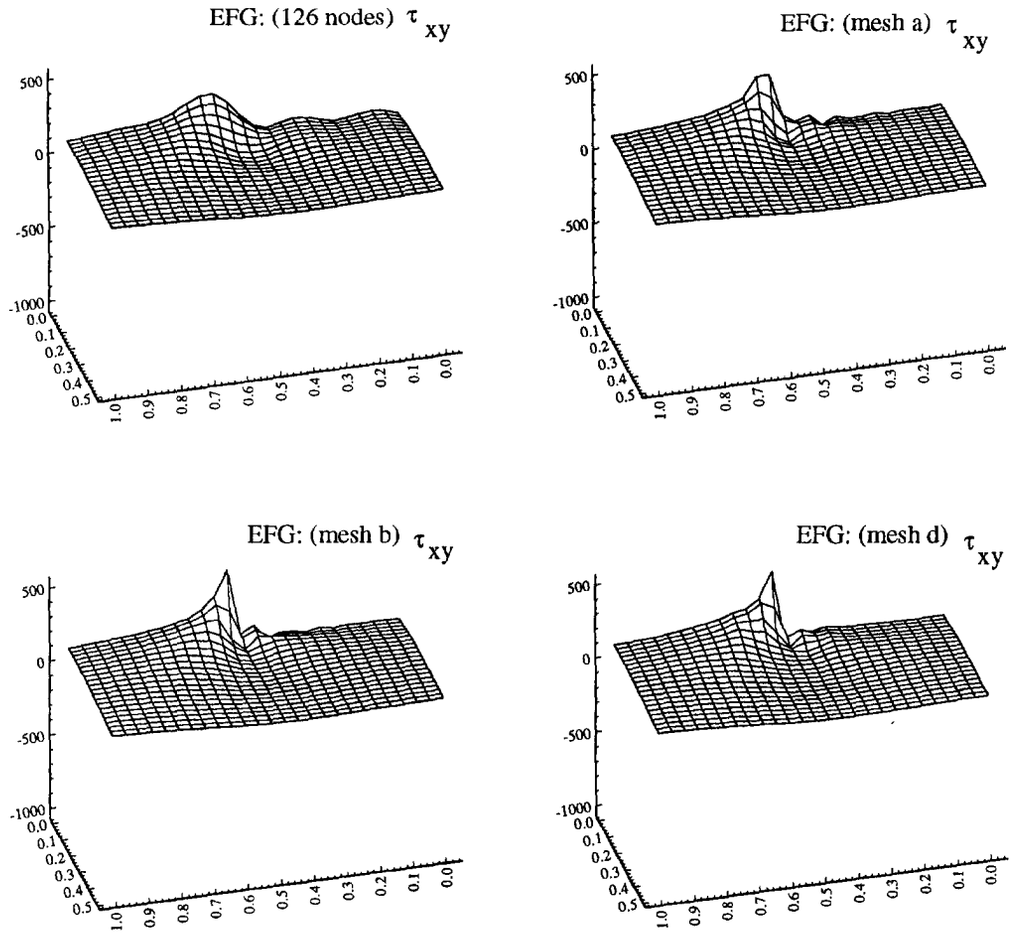

Fig. 5. Shear stress distributions ($y > 0$) for the coarse meshes in the near-tip mixed-mode crack problem.

calculation is that it predicts crack bridging in a manner that is similar to that often observed. However, it should be noted that the computation in the last steps of the process are undoubtedly prone to error, for the stress intensity factor changes rapidly as the crack approaches the free surface. This stage of the problem is now under further study, with the aim of discerning whether the phenomena noted in the last stages of crack bridging can indeed be replicated by this method.

Contour plots for the effective stress in two stages of crack growth are given in Fig. 10. The stress concentration at the crack tip can clearly be discerned. We remark that the piecewise linear character of the contours is not a true representation of the EFG solution. Since we have not yet developed a post-processor for the EFG method, a finite element contour plotter TECPLOT was used which performed a Voronoi triangulation of the nodes prior to plotting. Hence the contours appear to be piecewise linear rather than smooth as they are with the MLS interpolants.

The crack growth for the larger initial angle (i.e. $\theta = 45^\circ$) is summarized briefly in Fig. 11, which shows contour plots for the stresses at two stages of the computation. In this case, no crack bridging occurs: the cracks clearly pass by each other like two strangers in the night. Note that the crack line has been enhanced in the figures because after conversion of the color contour plots to black and white, the crack was no longer clearly visible.

The next set of examples involve the simulation of cracks in a dynamic field, where the inertia term in eqn (26) was included. All calculations were performed by the central difference, explicit method with a diagonal mass matrix. The first example is a stationary edge crack in a two-dimensional solid in plane strain subjected to a mixed-mode dynamic

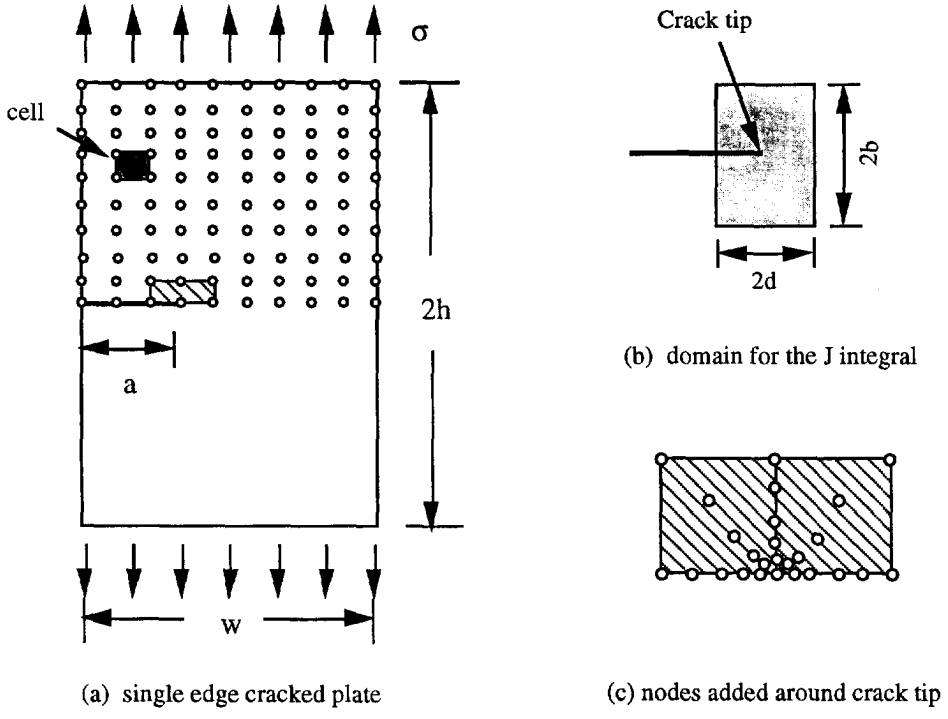

Fig. 6. Problem statement for a single plate with edge crack.

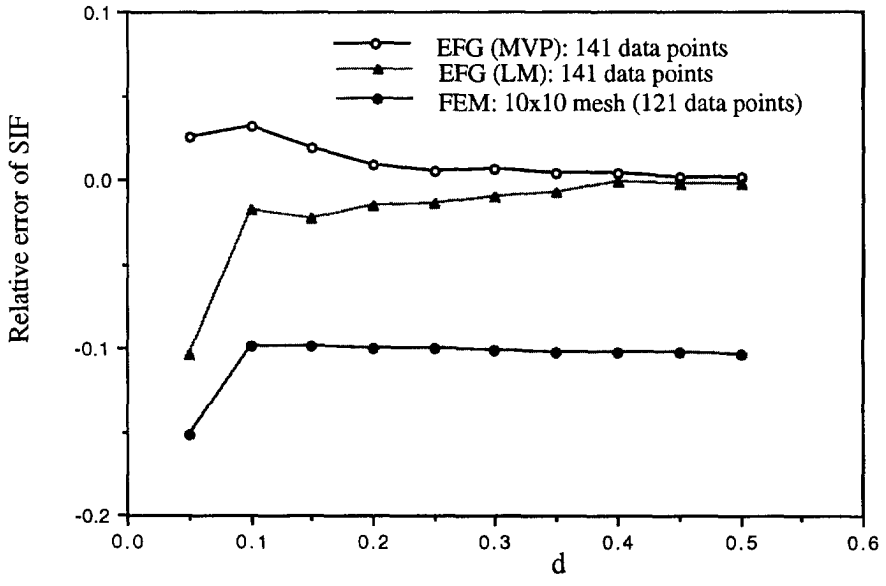

Fig. 7. Relative errors of different integration domains on accuracy of stress intensity factor ($b/d = 2$).

loading as shown in Fig. 12. The elastic constants and problem parameters are $E = 211.0 \times 10^3$, $\rho = 0.78 \times 10^{-3}$, $\nu = 0.25$, $a = 1$ (crack length) and $v_0 = 16.5$. The nodes used in the calculation were shown in Fig. 11. The analytical solution has been found in a pioneering paper by Lee and Freund (1990). The body is initially at rest and a constant velocity v_0 is applied as a step function at $t = 0$ on the boundary of the plate on one side of the edge crack. As a result of the loading, a compression wave propagates towards the crack tip and relatively large shear stresses are induced on the crack around the crack tip resulting in mixed-mode fracture behavior.

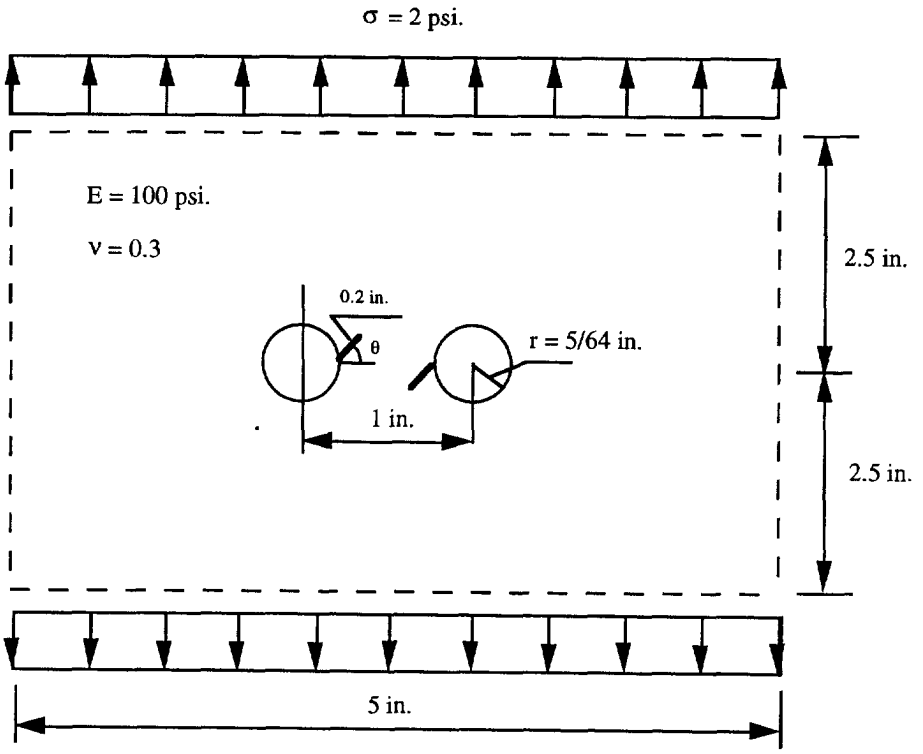

Fig. 8. Statement of the fatigue crack growth problem.

The number of cells was 20×20, and 3×3 Gauss quadrature was used in all cells except those around the crack tip, where 5×5 Gauss quadrature was used. The time step was calculated automatically in the program by using the stability condition (35). The time histories of the normalized stress intensity factors are shown in Fig. 13; they show good agreement with the analytical solution of Lee and Freund (1990). The stress intensity factors K_{I} and K_{II} were calculated by conservation integrals which directly evaluate the individual stress intensity factors for the mixed-mode crack problem in terms of known auxiliary solutions (Yau *et al.*, 1980). The contour integrals were also converted into domain integrals.

To conclude, we consider dynamic problems with a growing crack. The attractiveness of the EFG is that the moving crack is simply modeled as a line. As this line extends, sampling points along the path of the crack will lose nodes from their list of neighbors. For example, consider two cells with six nodes and 6×6 Gauss quadrature points in each cell around the crack tip as shown in Fig. 14. The crack is represented by two solid lines intersecting at the crack tip [Fig. 14(a)]. As the crack moves the lines extend as shown in Fig. 14(b). Gauss quadrature point "q" will lose nodes 1, 2 and 3 from its domain of influence because they are on the other side of the crack.

Consider a semi-infinite crack in an infinite body subjected to a pulse of magnitude σ_0 parallel to the crack plane. The body is under plane strain conditions with elastic constants $E = 211$ GPa, $\nu = 0.30$ and $\rho = 7800$ kg m^{-3}. The dilation, shear and Rayleigh wave speeds are denoted as c_{d}, c_{s} and c_{r}, respectively. At time $t = 0$, the wave front reaches the crack plane; subsequently at $t = \tau$, the crack is assumed to grow at a constant speed, v. The analytical solution for the dynamic stress intensity factor is independent of τ as shown by Freund (1990):

$$K(t, v) = k(v)K(t, 0). \tag{42}$$

Here $K(t, 0)$ is the stress intensity factor for a stationary crack which for this specific case is given by:

$$K(t,0) = 2\sigma_0 \frac{\sqrt{[c_d t(1-2\nu)/\pi]}}{1-\nu}, \tag{43}$$

where $k(v)$ is a universal function of crack speed which, for the values of crack speed considered here, can be approximated by:

$$k(v) \approx \frac{1-v/c_r}{\sqrt{(1-v/c_d)}}. \tag{44}$$

The dynamic energy release rate is given by

$$G(t,v) = \frac{1-\nu^2}{E} A(v)[K(t,v)]^2, \tag{45}$$

where $A(v)$ is also a universal function of crack speed and is given by:

$$A(v) = \frac{v^2 \alpha_d}{(1-\nu)c_s^2 D} \tag{46}$$

$$D = 4\alpha_d\alpha_s - (1+\alpha_s^2)^2, \quad \alpha_d = \sqrt{(1-v^2/c_d^2)}, \quad \alpha_s = \sqrt{(1-v^2/c_s^2)}. \tag{47}$$

Equation (44) is applicable to crack growth in a bounded body as long as reflected waves from the boundaries do not reach the vicinity of the crack tip.

The model is a rectangular plate with an edge crack as shown in Fig. 15. The dimensions of the plate and crack are chosen such that within the time interval of interest reflected waves do not reach the crack tip region. The plate is initially at rest. A stress of magnitude σ_0 is applied as a step function in time to the upper edge in the y-direction; the remaining surfaces are traction free. No displacement boundary conditions appear in this model. A fixed time step of 0.5×10^{-5} was employed for a total of 180 time steps. The dynamic energy release rate $G(t,v)$ is calculated at each time step using the domain integral method with a square domain with sides of length 1.5 centered at the crack tip. The plate is descretized using square cells with a dimension of 0.05. Single point Gauss quadrature was used in all cells except those with centers inside a rectangle whose lower left corner is at (0, 1.9) and upper right corner is at (6.1, 2.05) (i.e. a rectangle enclosing the domain about the crack tip), where 8×8 Gauss quadrature was used.

In the calculation, the crack tip is assumed to move to the right with a constant velocity $0.4c_s$ after the compressive wave front arrives (i.e. $\tau = 1/c_d$). According to the closed form solutions of Freund (1990), the stress intensity factor then exhibits a step function decrease and begins growing again at a slower rate. As can be seen from Fig. 16, the computed results exhibit slight oscillations subsequent to the discontinuity in the time history, which occurs at the initiation of crack motion. However, in general good agreement is achieved between the computed and analytical results. Figure 17 shows part of the crack profile near the tip at the end simulation with displacements magnified by 10^4; nodes are shown as circles and Gauss points as dots. The crack tip has moved from $x = 5.0$ to $x = 5.74$, advancing through 14 cells.

The last example concerns a precracked specimen to which an initial impulse of 15 m s^{-1} is applied to the right-hand end, $x = 0$, $0 < y < 0.025$. The initial crack is at $y = 0.025$, $0 < x < 0.05$. The line $y = 0$ is a line of symmetry. The final configuration of the crack is shown in Fig. 18; the domains used for the evaluation of the stress intensity factors is also indicated. In the experiment which is being modeled, the crack propagated at an angle of about 67°. In the EFG model, the crack propagation is somewhat irregular but the approximate angle from the root of the crack to the tip is about 70°.

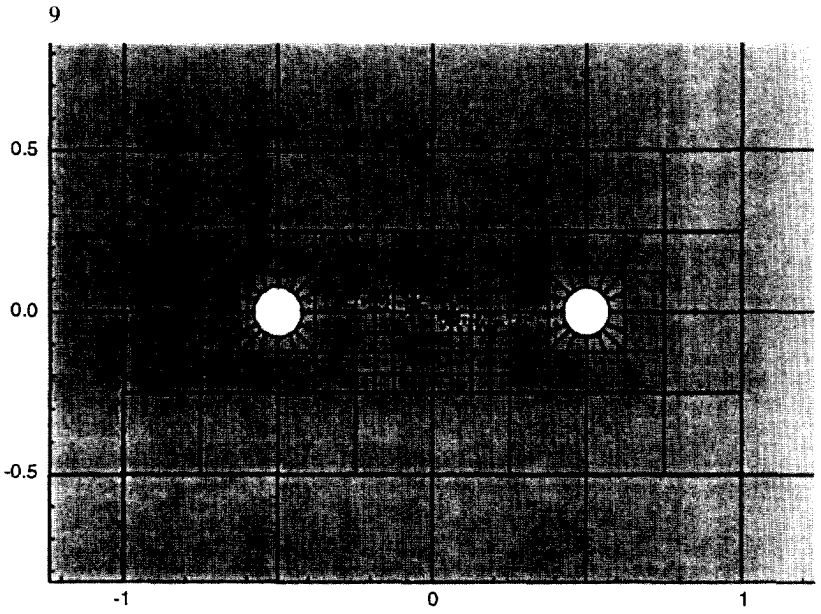

Fig. 9. Cell structure and nodal arrangements for the crack with $\theta = 10^{\circ}$ after three steps.

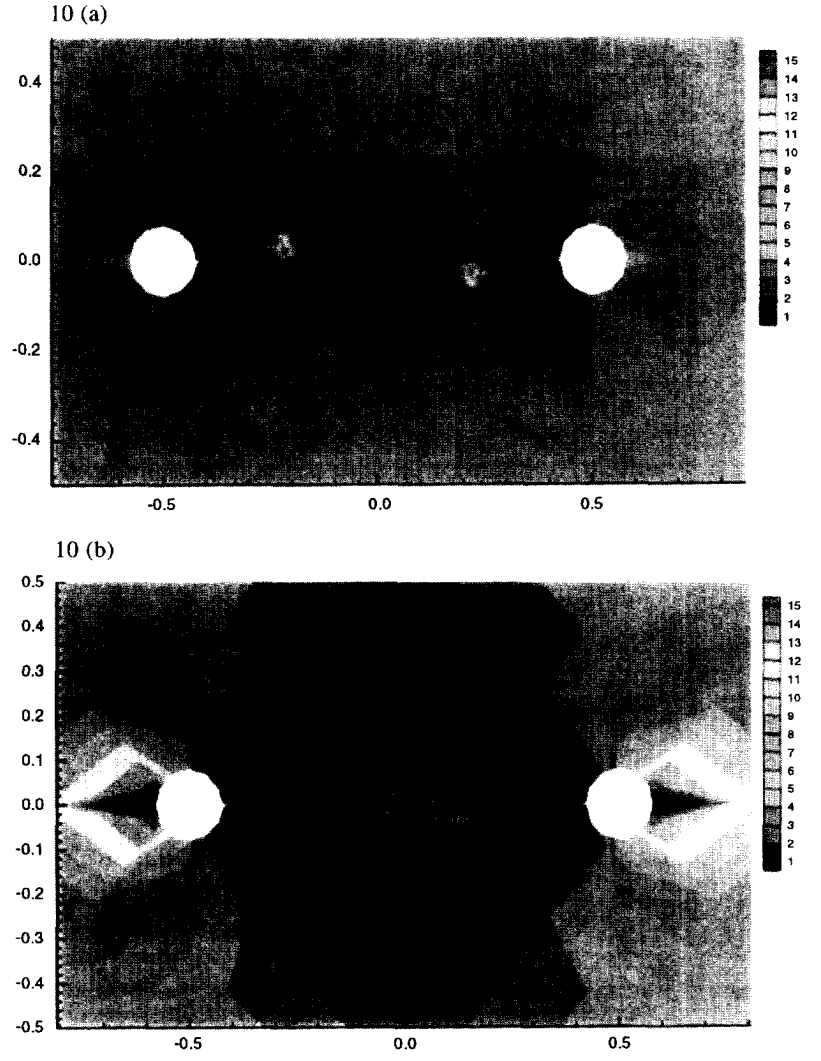

Fig. 10. (a) Effective stress in crack growth for $\theta = 10^{\circ}$ in the initial state. (b) Effective stress in crack growth for $\theta = 10^{\circ}$ after nine steps.

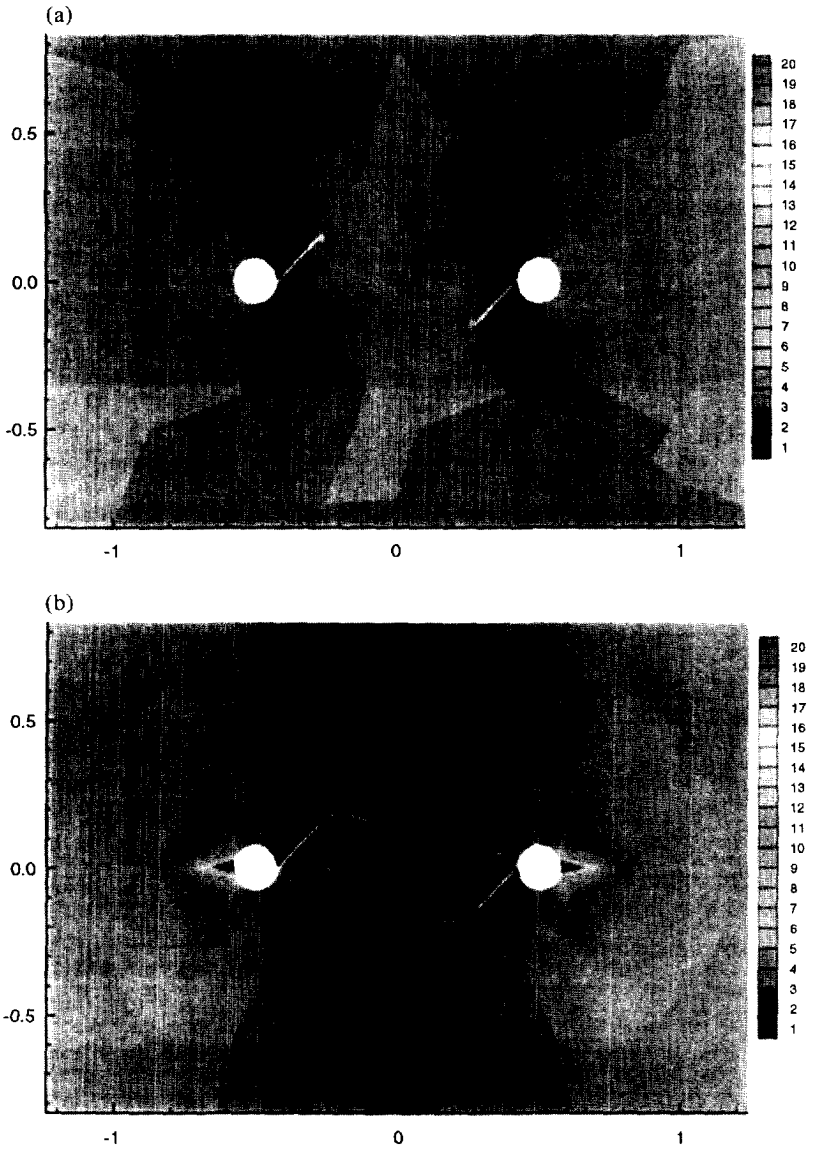

Fig. 11. (a) Effective stress in crack growth for $\theta = 45^\circ$ in the initial state. (b) Effective stress in crack growth for $\theta = 45^\circ$ after 17 steps.

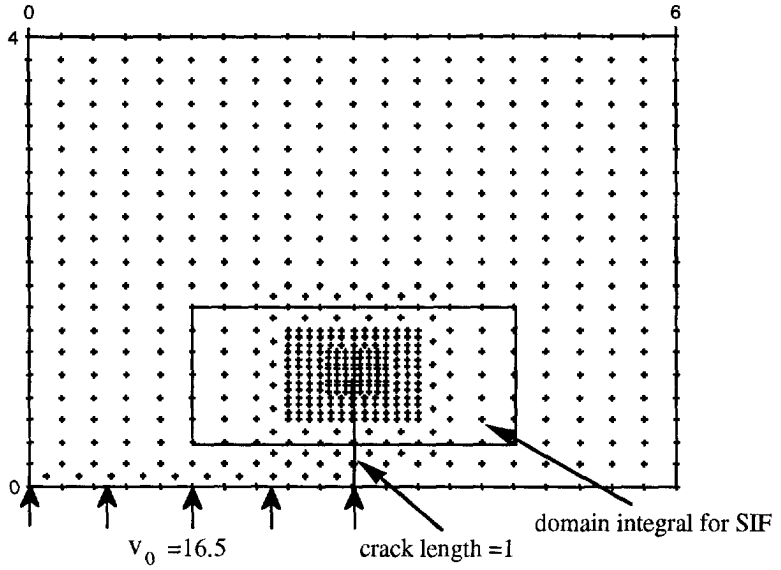

Fig. 12. Problem statement and nodes for the stationary crack under dynamic loading.

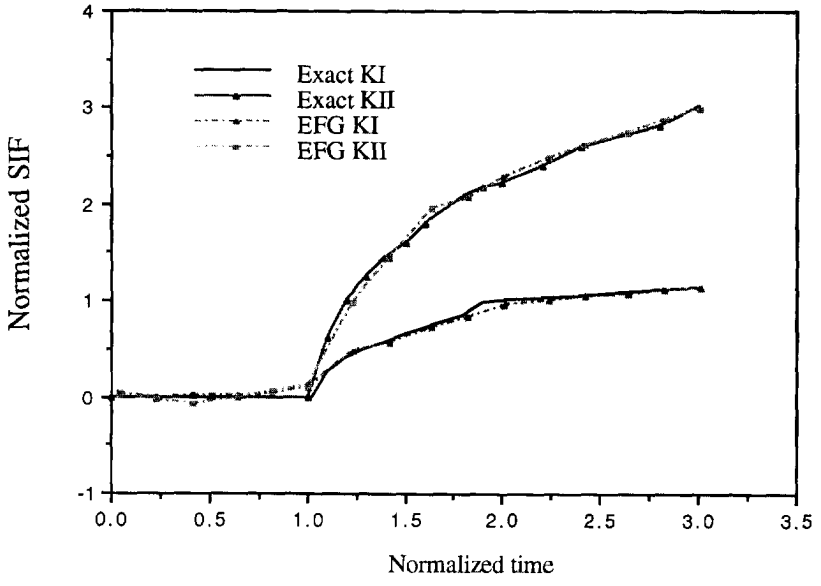

Fig. 13. A comparison of analytical and numerical results for the time history of stress intensity factors in the stationary crack problem.

5. CONCLUSIONS

The capability of the EFG method to model the evolution of growing cracks has been demonstrated in both static and dynamic examples. In both cases, a growing crack can be modeled simply by extending the free boundaries associated with the crack. In contrast to finite element methods, it is not necessary to remesh or to use arbitrary Lagrangian Eulerian formulations, although the addition and motion of nodes is advantageous for static problems.

The versatility of the method does entail additional computational costs, which range from moderate in the static problems to substantial in the dynamic problems. The main cost burden arises from the need to find the nodes within the domain of influence of each quadrature point. In the static problems, because of their moderate size and the fact that most of the computational effort is devoted to equation solving, the increase in solution time compared with finite element methods is moderate (of the order of 50%). On the other

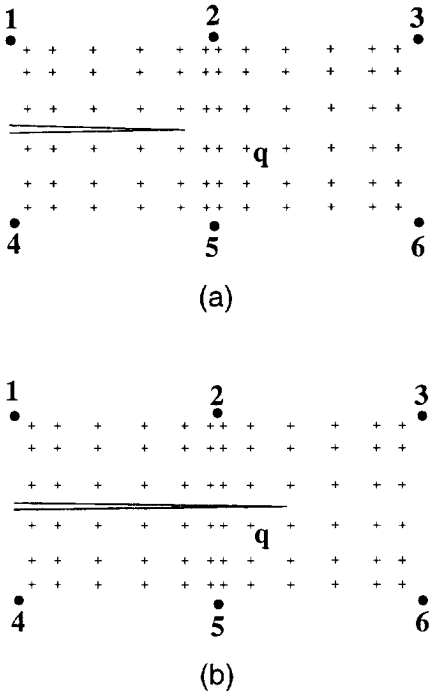

Fig. 14. Crack advancing through two cells with 6×6 Gauss quadrature points. Quadrature point "q" which was not affected by the crack in (a) will lose nodes 1, 2 and 3 from its domain of influence as the crack extends in (b).

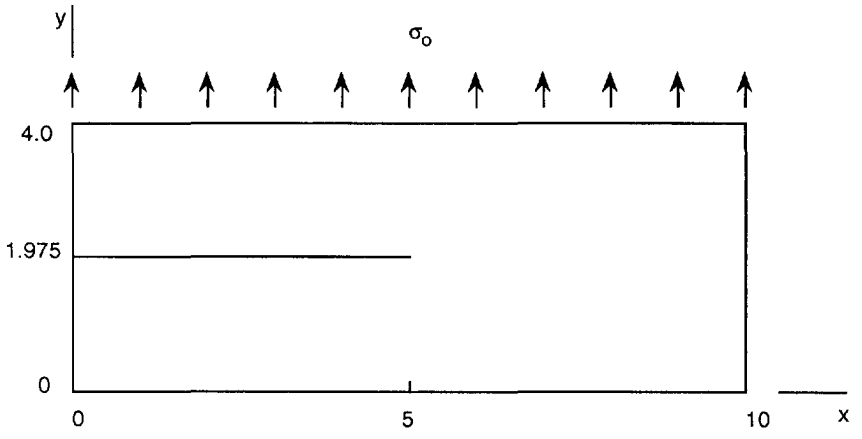

Fig. 15. Plate under plane strain conditions subjected to a stress of magnitude σ_0 applied as a step function in time. The initial crack is at $y = 1.975$ and extends from $x = 0$ to $x = 5$.

hand, in the dynamic problems, the additional burden of the nodal search in the present calculation was substantial, even if it was limited to the vicinity of the crack tip. Nevertheless, with the increasing speed of computers, the cost is trivial compared with what would be required in terms of man time to remesh these problems.

The strategies that we recommend for static and dynamic problems are quite different. In static problems, it appears to be best to configure the arrangement of nodes in conformance with the geometry of the evolving crack. It is beneficial to place nodes along both sides of the edge of the crack and to maintain a dense set of nodes around the crack tip. The latter is very effective in enhancing the accuracy of the computed stress intensity factors. The results presented here show that by modeling crack growth by extending the free

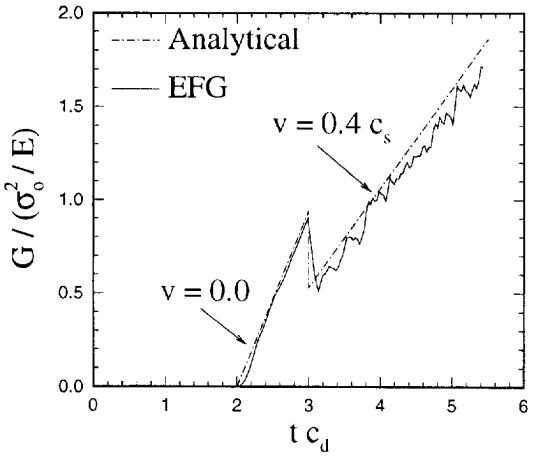

Fig. 16. Comparison of the normalized energy release rate G as determined from the plate shown in Fig. 15 with the analytical solution given in eqn (41). For the case of $v = 0.4c_s$, crack propagation starts at $t > 3\ c_d$.

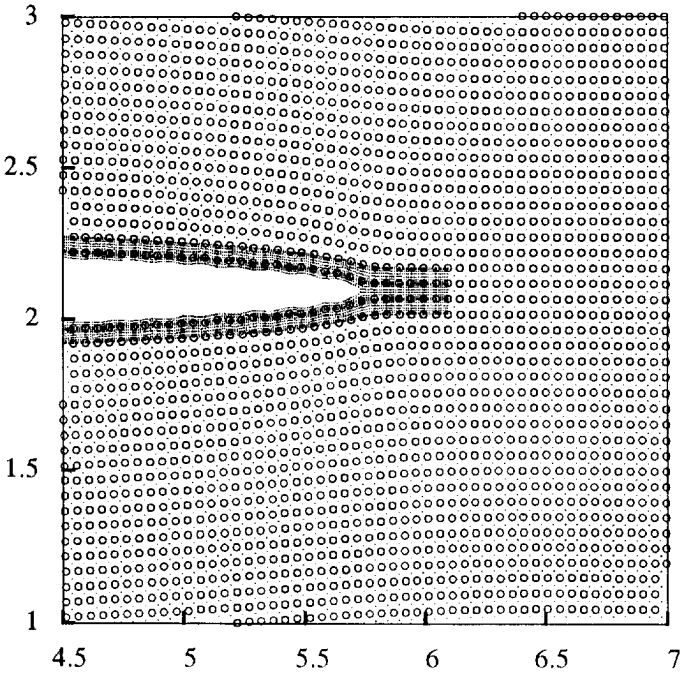

Fig. 17. Profile close to the crack tip at the end of simulation with displacements magnified by 10^4. The crack has moved from $x = 5.0$ to $x = 5.74$ advancing through 14 cells. Circles and dots represent nodes and Gauss points, respectively.

boundaries and moving the nodes with the crack tip, accurate mode I and mode II stress intensity factors can be computed by the EFG method in static crack growth problems. Since moving the nodes in static elastic problems is straightforward, this approach is very promising for problems with complex static patterns of crack growth such as occur in fatigue problems. The addition and motion of nodes is much simpler than remeshing in finite element methods because no element connectivities need to be established; the coordinates of the nodes and the geometric descriptions of the boundaries, both exterior and those arising from the crack, suffice to describe the entire numerical model.

In dynamic problems, the approach of reconfiguring the mesh with the evolution of the crack is not recommended. The shortcomings of this approach are twofold:

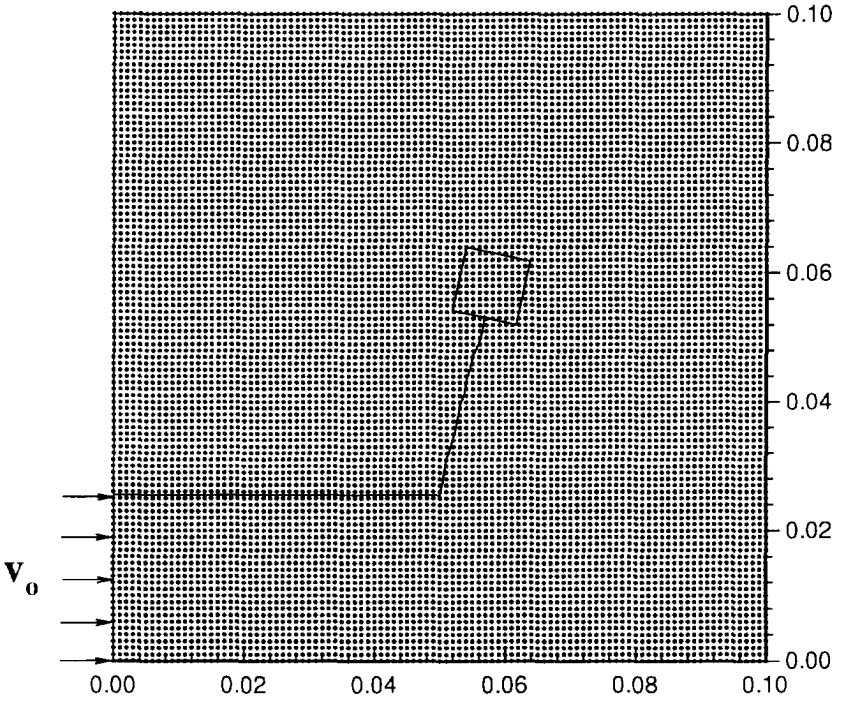

Fig. 18. Mesh for an initially precracked specimen showing the crack emanating from the tip of the initial crack and the domain used for evaluation of the stress intensity factors; the initial crack lies along the axis of symmetry.

(1) the resulting arrangements of nodes are inadequate for resolving the waves which occur in the interior of the body and which are crucial to computing accurate stress intensity factors;

(2) the motion of nodes introduces substantial changes in the dependent variables, which introduces errors in time-dependent evolution problems such as elastodynamics. We do not yet know what the optimal strategy will be for more weakly history-dependent problems such as static, elastoplastic crack growth, for in that case the history dependence arises primarily from the history of the yield function and changes in the fields due to nodal motions are not likely to be as severe as in dynamics.

The dichotomy in strategies for the two classes of problems arises from two reasons:

(1) the static, elastic problems are treated by direct solvers such as Cholesky decomposition, so eliminating as many extraneous nodes as possible is advantageous since the cost depends on n^2 where n = number of nodes (for banded systems), whereas the dynamic problems have been treated by explicit integration, where the cost varies linearly with the number of nodes n (since the stable time step is not reduced by filling in nodes);

(2) the dynamic problem is hyperbolic, so the support of the weight functions cannot be very large.

There are still many aspects of the EFG method which need refinement and understanding: what are the underlying factors which determine the rate of convergence for elliptic and hyperbolic problems? Why is the domain integral not as size-independent as it is in the finite element method? What is the best strategy for numerical integration? (Obviously the uniform background cells used originally in the EFG method will not suffice for more complex geometries.)

Nevertheless, our experience with the method so far indicates that the method has considerable promise in dealing with complex problems of crack propagation in both static and dynamic conditions.

Acknowledgements—The support of the Air Force Office of Scientific Research and the Office of Naval Research to Northwestern University is gratefully acknowledged.

REFERENCES

Ando, Y., Yagawa, G. and Sakai, Y. (1975). In *Transactions of the 3rd International Conference on SMIRT*, London Paper L 7/1.

Aoki, S., Kishimoto, K. and Sakata, M. (1987). Finite element computation of dynamic stress intensity factor for a rapidly propagating crack using $\tilde{J}$-integral. *Comput. Mech.* **2,** 54–62.

Atluri, S. N. and Nishioka, T. (1985). Numerical studies in dynamic fracture mechanics. *Int. J. Fracture* **27,** 245–261.

Bazzard, R. J., Gross, B. and Srawley, J. E. (1986). Mode II fatigue crack growth specimen development. *ASTM STP* **905,** 329–346.

Belytschko, T., Lu, Y. Y. and Gu, L. (1993). Crack propagation by element-free Galerkin methods. *Engng Fracture Mech.* In press.

Belytschko, T., Gu, L. and Lu, Y. Y. (1994a). Fracture and crack growth by element-free Galerkin. *Modelling Simulation Mater. Sci. Engng.* **2,** 519–534.

Belytschko, T., Lu, Y. Y. and Gu, L. (1994b). Element-free Galerkin methods. *Int. J. Numer. Meth. Engng* **37,** 229–256.

Broek, D. (1982). *Elementary Engineering Fracture Mechanics*. 3rd Ed. Martinus Nijhoff.

Cormen, T. H., Leiserson, C. E. and Rivest, R. L. (1990). *Introduction to Algorithms*. McGraw-Hill, New York.

Crowley, W. P. (1985). Free-Lagrange methods for compressible hydrodynamics in two space dimensions. In *The Free-Lagrange Method* (Edited by M. J. Fritts, W. P. Crowley and H. E. Trease). Springer, New York.

Erdogan, F. and Sih, G. C. (1963). On the crack entension in plates under plane loading and transverse shear. *ASME J. Basic Engng* **85.**

Freund, L. B. (1990). *Dynamic Fracture Mechanics*. Cambridge University Press, Cambridge.

Gingold, R. A. and Monaghan, J. J. (1977). Smoothed particle hydrodynamics: theory and application to non-spherical stars. *Mon. Not. R. Astron. Soc.* **181,** 375–389.

Hussain, M. A., Pu, S. L. and Underwood, J. H. (1974). Strain energy release rate for a crack under combined Mode I and Mode II. *Fracture Analysis. ASTM STP* **560.**

Hughes, T. J. R. (1987). *The Finite Element Method*. Prentice-Hall, Englewood Cliffs, New Jersey.

Johnson, G. R., Peterson, E. H. and Stryrk, R. A. (1993). Incorporation of an SPH option into the EPIC code for a wide range of high velocity impact computations. In *A Colloquium on Advances in Smoothed Particle Hydrodynamics*.

Kobayashi, A. S., Emery, A. F. and Mall, S. (1976). Dynamic-finite-element and dynamic-photoelastic analyses of two fracturing Homalite-100 plates. *Exp. Mech.* **16,** 321–328.

Koh, H. M., Lee, H. S. and Haber, R. B. (1988). Dynamic crack propagation analysis using Eulerian–Lagrangian kinematic descriptions. *Comput. Mech.* **3,** 141–155.

Lancaster, P. and Salkauskas, K. (1981). Surfaces generated by moving least squares methods. *Math. Comput.* **37,** 141–158.

Lancaster, P. and Tismenetsky, M. (1985). *The Theory of Matrices*. Academic Press, London.

Lee, Y. J. and Freund, L. B. (1990). Fracture initiation due to asymmetric impact loading of an edge cracked plate. *J. Appl. Mech.* **57,** 104–111.

Li, F. Z., Shih, C. F. and Needleman, A. (1985). A comparison of methods for calculating energy release rates. *Engng Fracture Mech.* **21,** 405–421.

Lu, Y. Y., Belytschko, T. and Gu, L. (1994a). A new implementation of element-free Galerkin methods. *Comput. Meth. Appl. Mech. Engng.* **113,** 397–414.

Lu, Y. Y., Belytschko, T. and Tabbara, M., (1994b). Element-free Galerkin methods for wave propagation dynamic fracture. To be published in *Comput. Meth. Appl. Mech. Engng.*

Lucy, L. (1977). A numerical approach to testing the fission hypothesis. *A. J.* **82,** 1013–1024.

Malluck, J. F. and King, W. W. (1978). *Numerical Methods in Fracture Mechanics* (Edited by A. R. Luxmoore and D. R. J. Owen). Swansea, U.K.

Moran, B. and Shih, C. F. (1987a). Crack tip and associated domain integrals from momentum and energy balance. *Engng Fracture Mech.* **27,** 615–642.

Moran, B. and Shih, C. F. (1987b). A general treatment of crack tip contour integrals. *Int. J. Fracture* **35,** 295–310.

Nayroles, B., Touzot, G. and Villon, P. (1992). Generalizing the finite element method: diffuse approximation and diffuse elements. *Comput. Mech.* **10,** 307–318.

Rashid, Y. R. (1968). Analysis of prestressed concrete vessels. *Nuclear Engng Design* **7,** 334–355.

Sih, G. C. (1974). Strain-energy-density factor applied to mixed-mode crack problems. *Int. J. Fracture Mech.* **10**(3).

Smith, C. W. and Wiersma, S. J. (1986). Stress-fringe singnatures for propagating crack. *Engng Fracture Mech.* **23,** 229–236.

Shepard, D. (1968). A two-dimensional interpolation function for irregularly spaced points. *Proceedings of the A.C.M. National Conference*, pp. 517–524.

Trease, H. E. (1985). Three-dimensional free Lagrangian hydrodynamics. In *The Free-Lagrange Method* (Edited by M. J. Fritts, W. P. Crowley and H. E. Trease). Springer, New York.

Wawrzynek, P. A. and Ingraffea, A. R. (1987). Interactive finite element analysis of fracture processes: an integrated approach. *Theor. Appl. Fracture Mech.* **8**, 137–150.

Yagawa, G., Sakai, Y. and Ando, Y. (1977). Fast fracture and crack arrest. (Edited by G. T. Hahn and M. F. Kanninen). *ASTM* **627**, 109–122.

Yau, J. F., Wang, S. S. and Corten, H. T. (1980). A mixed-mode crack analysis of isotropic solids using conservation laws of elasticity. *J. Appl. Mech.* **47**, 335–341.